# Magnetic properties of Fe films on flat and vicinal Au(111): Consequences of different growth behavior

T. Allmers[*] and M. Donath

*Physikalisches Institut, Westfälische Wilhelms-Universität Münster, Wilhelm-Klemm-Str. 10, 48149 Münster, Germany*

The epitaxial growth of Fe on flat Au(111) differs from Fe on vicinal Au(111). One consequence is a different critical Fe overlayer thickness at which a structural phase transition from fcc(111) to bcc(110) takes place. The critical thickness is higher for Fe on vicinal Au(111) than on flat Au(111). Accompanied with the structural phase transition is a spin-reorientation transition of the easy-magnetization direction from out of plane to in plane. In agreement with the impeded phase transition we observe an impeded spin-reorientation transition on vicinal Au(111). The spin-reorientation transition, however, proceeds in a narrow coverage range while the structural phase transition occurs gradually over a larger thickness range. A further consequence of the different growth behavior is a different topography for thicknesses beyond the phase transition. Fe on flat Au(111) exhibits a sixfold symmetry, Fe on vicinal Au(111) only a twofold symmetry. The different symmetries influence the magnetic properties: while for bcc Fe(110) on flat Au(111) no easy-magnetization direction could be determined, we identified a preferred direction for Fe on vicinal Au(111) which is perpendicular to the step edges. The twofold symmetry causes an uniaxial magnetic behavior. This knowledge of the magnetization behavior is essential for correctly analyzing spin-resolved measurements of the electronic structure as demonstrated by photoemission measurements.

## I. INTRODUCTION

The preparation of nanostructures is a highly topical issue in solid-state physics. Various techniques have been developed to fulfill this task throughout the last decades.[1] One successful approach is the fabrication of nanostructures by self-structuring methods because it provides such a parallelism that cannot be achieved by conventional bottom-up or top-down approaches. Besides other self-structuring approaches, vicinal surfaces attracted much interest as templates for the production of one-dimensional nanostructures due to a repulsive step-step interaction which generates a regular array of steps on the surface.[2] In case, the deposited material grows in a step-flow-growth mode, the regular array of the template is preserved and a regular array of nanostructures is formed.[3] The existence of such a regular array is also necessary when using characterization techniques which are spatially integrating like direct and inverse photoemission. In this way several research groups have already successfully produced nanostructures ranging from monatomic chains to wide stripes.[4–13] The distance of the wires and stripes can be tuned by varying the step density, i.e., changing the miscut angle of the crystal.

For the fabrication of magnetic nanostructures it may be helpful to use wide terraces in order to grow wide detached stripes. This approach helps to overcome the (super)paramagnetic limit for a given temperature. The terrace width of the surface cannot be increased arbitrarily because the repulsive step-step interaction decreases with the square of the distance to the step edges. This causes the steps to meander and the spacing between the step edges becomes irregular.[2] Thus, the regular step array is no longer preserved on the template. This problem is less crucial for vicinal Au(111) surfaces: some vicinal Au(111) surfaces exhibit large, regular, and reconstructed terraces, which are stable against facetting.[14] The terrace width distribution is very narrow compared with other metallic surfaces and about two or three times smaller than for vicinal Cu(111) with comparable terrace width.[15,16] This reflects a strong repulsive step-step interaction resulting probably from the surface reconstruction.

In a previous work we found significant differences between the growth behavior of Fe on flat Au(111) and the vicinal surface Au(23 25 25) (Ref. 17) which may influence the magnetic properties of the film. We found that the structural phase transition from fcc(111) to bcc(110) is impeded for Fe on Au(23 25 25) in comparison with Fe on flat Au(111). Since the structural phase transition is accompanied by a spin-reorientation transition (SRT) from out of plane to in plane, we expect that the SRT is also impeded for Fe on vicinal Au(111). A further difference is the orientation of the bcc(110) Fe crystallites which are formed as a result of the phase transition: while the crystallites on flat Au(111) are elongated in all $\langle 01\bar{1}\rangle_{\text{fcc}}$ directions, the crystallites on vicinal Au(111) are only present along $[\bar{1}01]_{\text{fcc}}$ and $[\bar{1}10]_{\text{fcc}}$.

Due to the missing growth along $[01\bar{1}]_{\text{fcc}}$ this results in a reduced, twofold symmetry for Fe on Au(23 25 25) in comparison with a sixfold symmetry for Fe on flat Au(111). We expect a different in-plane magnetization behavior for these two systems due to the different symmetries. It is known from the literature that ultrathin films can exhibit an uniaxial magnetic anisotropy when deposited onto a vicinal substrate owing to the altered symmetry by the step array.[18–22] The induced easy-magnetization direction is either parallel or perpendicular to the step edges depending on the nontrivial interplay of various anisotropy contributions. The size of the individual contributions is influenced by both the geometry and crystalline properties of the deposited nanosized structures and details of the vicinal substrate, including miscut angle, coordination number of the step atoms, and electronic

interaction between substrate and overlayer. We will come back to this point when we discuss our results.

This paper is organized as follows: beside the experimental details given in Sec. II we describe in detail how the thickness of the Fe film was calibrated. In Sec. III A we present our magneto-optical Kerr-effect (MOKE) results concerning the SRT of Fe on flat and vicinal Au(111). Section III B compares the in-plane magnetization behavior of Fe on flat and vicinal Au(111) monitored with MOKE and spin-resolved photoemission (PE). With the results obtained we are able to deduce an easy-magnetization direction for Fe on vicinal Au(111). A summary of the results will be given in Sec. IV.

## II. EXPERIMENTAL DETAILS

The experiments were performed in a multifunction ultrahigh-vacuum (UHV) apparatus equipped with various techniques. Details are given in Ref. 23.

The MOKE setup is homemade. The sample is illuminated at 45° with polarized light from a HeNe laser ($\lambda$ =632.8 nm). A good signal-to-noise ratio is achieved by applying a photoelastic modulator combined with lock-in technique. The maximum field strength applied for in-plane measurements is 700 Oe and for out-of-plane measurements 470 Oe. The vicinal Au(111) sample was mounted on a turnable sample holder. The sample can be turned *in situ* stepless up to 90°. Therefore, the field can be applied along and perpendicular to the step edges of the substrate during MOKE measurements.

The PE data were obtained using a 50 mm simulated hemispherical sector analyzer (SHA50 from Focus GmbH). For spin-resolved PE, a spin-polarized low-energy electron-diffraction (LEED) detector was employed.[24,25] For excitation a helium discharge lamp was used providing unpolarized He-I light with an energy of $\hbar\omega$=21.22 eV.

After introducing the Au(111) sample into the UHV chamber, the sample was sputtered with 600 eV Ar$^+$ ions and subsequently annealed to 1000 K in order to restore crystallographic order. The sputtering and annealing cycles were repeated until no contamination was detected with Auger-electron spectroscopy (AES) within the detection limit [1–5 % of a monolayer (ML) depending on the impurities]. At this point a $(1 \times 1)$-LEED pattern was observed superimposed by additional spots from the Au(111) surface reconstruction.[26,27] The scanning tunneling microscopy (STM) measurements showed the characteristic herringbone reconstruction.[28,29] We observed terrace widths of more than 200 nm.

The vicinal Au(111) sample was prepared *extra situm* by polishing the crystal under a miscut angle of 2.3° toward the [$\bar{2}$11] direction (by the manufacturer MaTeck GmbH). After the sample was loaded into the UHV, the surface was sputtered with Ar$^+$ ions (600 eV) and subsequently annealed to 815 K in order to recover the thermodynamic stable crystallographic structure. A lower annealing temperature was applied to avoid the risk of destroying the regular step array. The sputtering and annealing cycles were repeated until no contaminations were detectable with AES and the LEED pat-

terns showed the characteristic splitting of the spots caused by the miscut angle (splitting perpendicular to the steps) and the surface reconstruction (splitting along the steps).[14] After more than a hundred sputtering and annealing cycles the STM measurements revealed straight and regular spaced monatomic high terraces which did not alter anymore by further preparation cycles. Due to the miscut of the crystal toward [$\bar{2}$11] the surface exhibits {111} microfacets with reconstructed terraces.[14] The reconstructed vicinal Au(111) surface shows discommensuration lines running perpendicular to the step edges in a "V" shape on the terraces.[14,30] These lines separate the fcc stacked regions from the fault stacked hcp regions. The average terrace width of the Au(23 25 25) surface is $\langle W \rangle$=(6.1 ± 0.8) nm and was determined by the examination of many STM measurements performed at different positions on the sample.[17] The Au(23 25 25) sample exhibits the same surface reconstruction and {111} microfacets as the Au(788) and Au(11 12 12) surfaces but has a significant larger terrace width.[14,17] The ratio of the Gaussian standard deviation and terrace width is 0.13 and about the same as for Au(788) and Au(11 12 12).[14,16,17]

To avoid possible contaminations from a crucible, Fe was evaporated from a high-purity rod by a water-cooled electron-beam evaporator. During evaporation the pressure was better than $5 \times 10^{-11}$ mbar.

Several methods were applied to calibrate the evaporation rate for Fe: (i) we used quantitative AES to calibrate the evaporation rate for Fe on Cu(001). In the literature it was reported that Fe grows not only layer by layer but also bilayer by bilayer. After the first one to two bilayers the growth proceeds layer by layer.[31,32] The initial growth behavior depends on the growth rate (layer-by-layer growth is present for low deposition rates while bilayer-by-bilayer growth is present for higher growth rates). With AES it is not easy to distinguish between layer-by-layer and bilayer-by-bilayer growth without further ado.

(ii) In order to determine which growth mode is present, we performed additional calibration measurements with MOKE. We used the well-studied transition of the easy-magnetization direction from out of plane to in plane between 10 and 12 ML (Ref. 33) in order to clarify whether we evaporated layer by layer or bilayer by bilayer on Cu(001).

(iii) In addition to AES and MOKE we determined the growth rate also with STM by measuring submonolayer Fe films deposited on Cu(001) and flat Au(111) at various positions on the sample.[17] The coverage was then determined using the scanning probe microscopy software WSXM.[34]

From our AES, MOKE, and STM results we found a layer-by-layer growth at a deposition rate of less than 0.1 ML/min for Fe on Cu(001) in contrast to a bilayer-by-bilayer growth at rates of more than 1 ML/min.[31,32] To favor a step-flow growth of Fe on the vicinal Au(111) surface a low deposition rate was chosen. During the evaporation of Fe the substrates were held at RT.

In the described calibration, ML was defined as the amount $N_{Fe}$ of Fe adatoms necessary to cover every atom of the Cu(001) substrate ($N_{Cu}$=15.3 atoms/nm$^2$). To use this result of the calibration for Fe on Au(111) in the same sense as described, the numbers of ML were multiplied
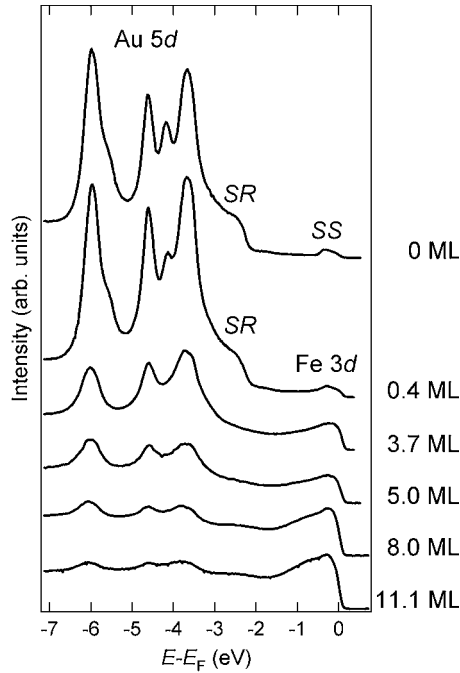
FIG. 1. Photoemission spectra from vicinal Au(111) measured for normal electron emission at RT (except for the coverage of 8.0 ML, which was measured at $T=145$ K) as a function of Fe overlayer thickness. The excitation energy was $\hbar\omega=21.22$ eV. In order to be able to compare the spectra with each other, they were normalized to equal background intensity.

by a factor of 1.11 for the coverage of Fe on Au(111) to take into account that the atomic density is 11% less ($N_{\mathrm{Au}}$ $=13.8$ atoms/nm$^2$).

(iv) We verified the results obtained with AES, MOKE, and STM by determining the electron attenuation length in Fe with PE. We measured Fe on flat and vicinal Au(111) for increasing overlayer thicknesses. The result of the PE measurements for Au(23 25 25) is shown in Fig. 1.

With increasing Fe coverage the intensities of the Au states are attenuated. The surface state (labeled $SS$) of Au(23 25 25) located at $E-E_{\mathrm{F}}=-0.4$ eV is reduced in intensity after deposition of Fe. The intensity increase right at $E_{\mathrm{F}}$ stems from Fe states. Consequently, the intensity at $E_{\mathrm{F}}$ increases with increasing Fe coverage. According to Yeh and Lindau,[35] the cross section for atomic Fe $3d$ orbits is 40 times larger than for atomic Fe $4s$ for an excitation energy of $\hbar\omega=21.22$ eV which was used throughout our PE experiments. Although the ratio of the cross sections is strictly speaking only correct for atoms and not for the solid state, the result suggests that the intensity of the spectral features stems mainly from Fe $3d$ states. At an energy of $E-E_{\mathrm{F}}=$ $-2.3$ eV a shoulder (labeled $SR$) is observed in the spectra for the clean surface and for the surface covered with 0.4 ML of Fe. This spectral feature is a surface resonance split off the bulk Au $5d$ states. The $SR$ is also reduced in intensity with increasing Fe overlayer thickness. The $SR$ is less sensitive toward the Fe adsorbate in comparison with $SS$ but significantly more sensitive than the bulk states. The slight increase at $E-E_{\mathrm{F}}\approx-2.3$ eV after the $SR$ is quenched is caused by the Fe states.[36]
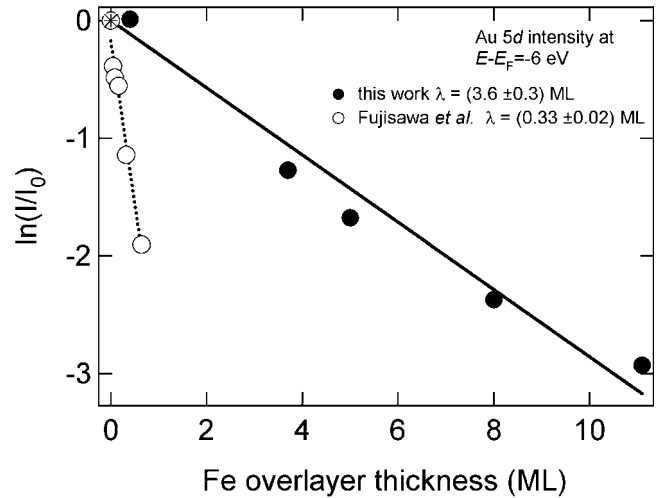


FIG. 2. Determination of the electron attenuation length $\lambda$ for Fe from the PE intensities of the Au $5d$ states at $E-E_{\mathrm{F}}\approx-6$ eV. The solid dots represent our measurements for the intensity of the Au $5d$ states with increasing Fe overlayer thickness. The solid line represents a linear fit through the data points from which $\lambda$ was determined. The empty dots are obtained from PE data taken by Fujisawa *et al.* (Ref. 37). The dotted line represents a linear fit through the data points. $\lambda$ is about an order of magnitude smaller in comparison with our result and other results in literature.

From the PE measurements we can deduce the electron attenuation length in Fe by comparing the intensity of the $5d$ bands for clean vicinal Au(111) and for various Fe overlayer thicknesses. The attenuation length $\lambda$ is given by

$$I(\Theta) = I_0 \times e^{-\Theta/\lambda},$$

where $I(\Theta)$ is the intensity of the Au $5d$ states at $E-E_{\mathrm{F}}\approx$ $-6$ eV for an overlayer thickness $\Theta$ and $I_0$ their intensity from the clean surface. To obtain the correct peak intensities, a linear background was subtracted. Figure 2 shows the natural logarithm of $I(\Theta)/I_0$ as a function of the Fe overlayer thickness. The solid dots show the results of our measurements. The solid line represents a linear fit through the data points from which $\lambda$ was determined. $\lambda$ is energy dependent[38] and the binding energy of 6 eV translates to a kinetic energy of $E\approx11$ eV. The electron attenuation length of Fe is therefore $\lambda(11\ \mathrm{eV})=(3.6\pm0.3)$ ML. Our result is in line with several values on various substrates.[39–41] The substrate does not alter the attenuation length of the overlayer. The results found for the attenuation length for Fe on flat Au(111) (not shown) are in agreement with the results found for Fe on vicinal Au(111).

However, one PE study in the literature points to a much smaller $\lambda$.[37] We deduced $\lambda$ from PE measurements by Fujisawa *et al.* for Fe on Au(788). The result are shown in Fig. 2 as empty dots. The dotted line represents a linear fit through the data points. For Fe, a $\lambda_{\mathrm{Fe}}(11\ \mathrm{eV})$ $=(0.31\pm0.01)$ ML is determined from the data in remarkable contrast to the value given above. The authors studied also the dependence of the electronic structure of Co and Ni on Au(788). For Co and Ni a $\lambda_{\mathrm{Co}}(11\ \mathrm{eV})$

TABLE I. The table gives the Fe overlayer thickness for which a SRT from out of plane to in plane and a structural phase transition from fcc(111) to bcc(110) was observed.

| Sample | SRT | Structural phase transition | Reference |
|---|---|---|---|
| Fe/Au(111) | 2.8 ML | 2.8 ML | 42 |
| | 3 Å | 3 ML | 43 |
| | 3.0–3.8 ML | see Table II | This work |
| [Fe/Au(111)]$_n$ | 4–6 Å | 10 Å | 44 |
| | 1–5 ML | N/A | 45 |
| Fe/Au(23 25 25) | 4.4–5.0 ML | see Table II | This work |

$=(0.24 \pm 0.02)$ ML and $\lambda_{Ni}(11 \text{ eV})=(0.28 \pm 0.02)$ ML are deduced from the data, which are also not in line with other measurements in the literature.[40]

We trust our thickness calibration for two reasons: first, the AES, MOKE, STM, and PE results agree with each other. Second, our results obtained with PE for the attenuation length of Fe agree with findings in the literature.

## III. RESULTS AND DISCUSSION

### A. Spin-reorientation transition of Fe on flat and vicinal Au(111)

The easy-magnetization direction changes from out of plane to in plane with increasing Fe film thickness. We performed MOKE measurements for Fe on flat and vicinal Au(111) to determine the critical Fe overlayer thickness at which the SRT takes place and correlated it to the structural phase transition. For Fe on flat Au(111) (not shown) we determined the SRT between 3.0 and 3.8 ML. No further SRT was observed up to 10 ML [highest coverage studied for the system Fe on flat Au(111) in this contribution]. This result agrees well with findings in the literature, as can be seen from Table I where the results of the critical Fe overlayer thickness of the SRT are compared with the Fe overlayer thickness of the structural phase transition for fcc(111) to bcc(110). The results of the polar MOKE measurements for Fe on vicinal Au(111) are shown in Fig. 3(a). The measurements were taken at $T=115$ K for various Fe overlayer thickness. At this temperature we observed a paramagnetic behavior for 1.1 ML of Fe. At a coverage of 1.4 ML of Fe a small hysteresis loop is present, indicating that the Curie temperature $T_C$ is above 115 K for this coverage. The shape of the hysteresis curve is not simply squarelike: the remanent magnetization is significantly smaller than the saturation magnetization. This shows that the temperature at which the measurements were conducted is too close to $T_C$ to neglect thermal fluctuations. A coverage of more than 1.7 ML Fe is necessary to observe a remanent magnetization nearly equal to the saturation magnetization at $T=115$ K. The hysteresis curves of more than 1.7 ML of Fe are also squarelike. The squareness of the hysteresis curves and the fact that the remanent magnetization equals the saturation magnetization are indications that the sample was magnetized along an easy-magnetization direction and that the magnetization does not
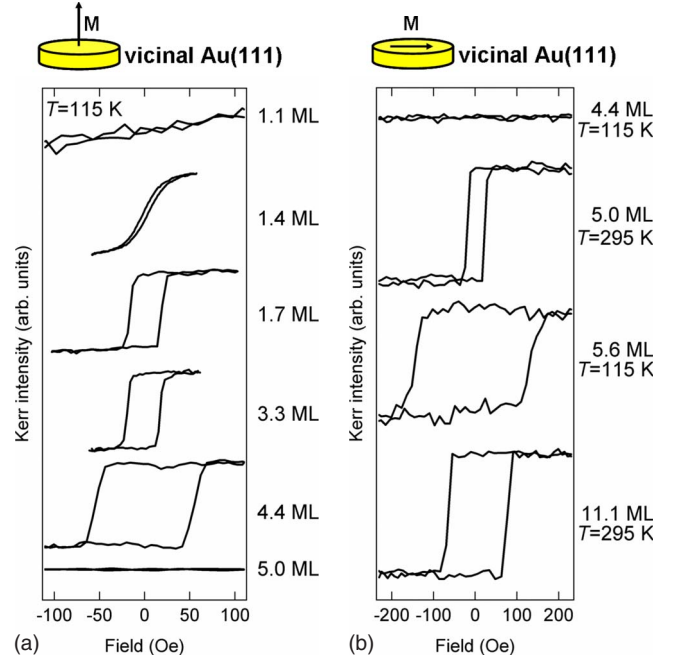


FIG. 3. (Color online) (a) Polar MOKE measurements performed at $T=115$ K for various Fe overlayer thicknesses on Au(23 25 25). At an overlayer thickness of 1.1 ML we observed a paramagnetic behavior of the Fe structures. For a coverage up to 4.4 ML the easy-magnetization direction is out of plane. (b) Result of the longitudinal MOKE measurements of different Fe overlayer thicknesses on Au(23 25 25). The measurements were performed at $T=115$ K and at $T=295$ K. Above 5 ML of Fe on Au(23 25 25) the easy-magnetization direction is in the film plane and stays in plane for the entire Fe overlayer thickness range studied. The magnetic field was applied perpendicular to the step edges. The sweeping speed of the field was about 5 Oe/s.

decay into domains. Furthermore, the temperature at which the data was obtained, seems to be sufficiently low with respect to $T_C$ that thermal fluctuations are negligible on the time scale used for our measurements (sweeping speed of the field: 5 Oe/s). For overlayer thicknesses of 5 ML and more we found no measurable polar Kerr signal. The easy-magnetization direction lies now in the film plane. The results of the longitudinal MOKE measurements are shown in Fig. 3(b). The field was applied perpendicular to the step edges of the substrate. The longitudinal MOKE measurements were performed at $T=115$ K and $T=295$ K. The influence of the temperature is clearly visible: the coercive field strength increases from 20 Oe for $T=295$ K (for 5.0 ML Fe) to 128 Oe for $T=115$ K (for 5.6 ML Fe). This effect is mainly due to the temperature-dependent anisotropy rather than the different coverage since the coercive field strength for 11.1 ML Fe at $T=295$ K (70 Oe) is again smaller than for 5.6 ML at $T=115$ K. The shape of the hysteresis curve of 5 ML and higher Fe coverage measured at $T=295$ K and $T=115$ K is similar to the shape of the hysteresis curve of 1.7 ML Fe measured at $T=115$ K indicating a complete switching of the magnetization along an easy-magnetization direction.

From the MOKE results we conclude that a SRT is taking place between 4.4 and 5.0 ML for Fe on vicinal Au(111). For

TABLE II. Summary of the results obtained with STM and LEED (Ref. 17) and MOKE.

| System | Fe/Au(111) (ML) | Fe/Au(23 25 25) (ML) |
|---|---|---|
| Appearance of crystallites in STM | 1.7 | 1.0 |
| Dominance of crystallites in STM | 3.0–3.3 | 3.7–5.0 |
| Start of satellite spot formation in LEED | >2.0 | >2.0 |
| End of satellite spot formation in LEED | 4.5 | 6.0 |
| Spin-reorientation transition in MOKE | 3.0–3.8 | 4.4–5.0 |

film thicknesses above the critical thickness the easy-magnetization direction stayed in plane to 20 ML [the highest coverage studied in this contribution for Fe on vicinal Au(111)].[46] The SRT is accompanied with a phase transition fcc(111) to bcc(110) (see Table I). We studied this structural phase transition in a former work with STM and LEED.[17] As can be seen from Table II, the results obtained from MOKE regarding the SRT correlate with the results obtained with STM and LEED for the structural phase transition.

We like to draw the reader's attention to two further aspects of the MOKE results: (i) in our MOKE study we were not able to observe a ferromagnetic behavior of Fe on vicinal Au(111) below 1.4 ML even at $T=115$ K. This result is at variance with to the results obtained by Fujisawa *et al.*,[37] who report a ferromagnetic behavior of individual Fe stripes of 0.6 ML Fe coverage for RT. A very recent publication by Shiraki *et al.*[47] confirms our results because they observed a

ferromagnetic behavior of 1 ML of Fe on Au(788) at $T=21$ K and a superparamagnetic behavior at $T=100$ K. The reason for the observed differences is the quite different thickness calibration by Fujisawa *et al.* as already shown in Sec. II.

(ii) Another interesting point is the observation that the SRT takes place in a narrow thickness range. Before and after the SRT we were not able to observe a measurable Kerr intensity for longitudinal and polar MOKE, respectively. This is worth to mention because the thickness range for the structural phase transition observed with STM and LEED is much wider (Table II). When comparing the MOKE and STM results we conclude that the SRT takes place when the bcc Fe(110) crystallites become dominant on the surface. Thus, the structural phase transition starts at different positions on the sample before the SRT occurs. A major part of the sample has to be transformed from fcc(111) to bcc(110) before the SRT takes place. Before and after the SRT the easy-magnetization direction of the sample seems to be governed by the fcc(111) or bcc(110) regions holding the majority. A coexistence of fcc(111) and bcc(110) Fe on Au(111) has not been reported so far but it is not unusual to observe fcc(111) and bcc(110) simultaneously. A system related to Fe on Au(111) is Fe on Cu(111): for the triangular islands, fcc Fe(111) regions were identified in the island center while bcc(110) regions are present at the rim of the islands.[48]

### B. Easy in-plane magnetization directions of bcc Fe(110) on flat and vicinal Au(111)

In this section we compare bcc Fe(110) on flat and vicinal Au(111). It is known that the structural phase transition fcc(111) to bcc(110) is accompanied by the formation of the
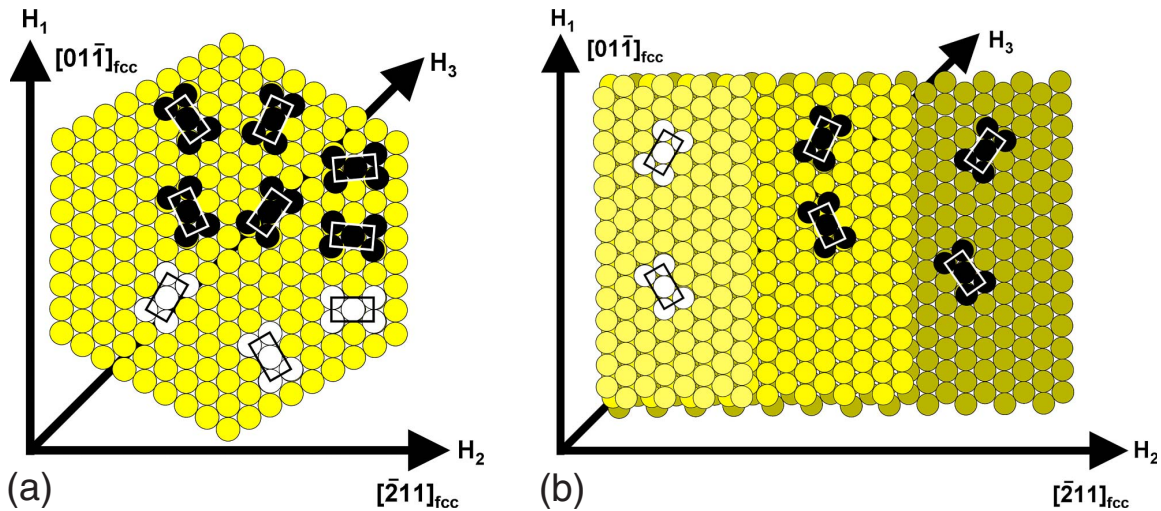


FIG. 4. (Color online) Illustration of the matching between the bcc(110) Fe unit cells on (a) flat and (b) vicinal Au(111). For simplicity the same lattice constant for Fe and Au was chosen. (a) For bcc(110) Fe six orientations of the unit cells are possible in the KS orientation (black atoms) and three orientations for the NW-growth mode (white atoms). (b) For bcc(110) Fe on Au(23 25 25), only two of three growth directions are found (Ref. 17): four orientations of the bcc(110) unit cells are possible in the KS mode (black atoms) and two in the NW mode (white atoms). The growth of the crystallites along the $[01\bar{1}]_{fcc}$ direction is not realized in the case of Fe/Au(23 25 25). This excludes the bcc(110) unit cells with an orientation of the $[001]_{bcc}$ parallel (NW mode) and close to parallel (KS mode) to $[01\bar{1}]_{fcc}$. Please note that the terrace width in this sketch was chosen to illustrate the orientations of the bcc(110) unit cells and does not correspond to the actual terrace width of Au(23 25 25).
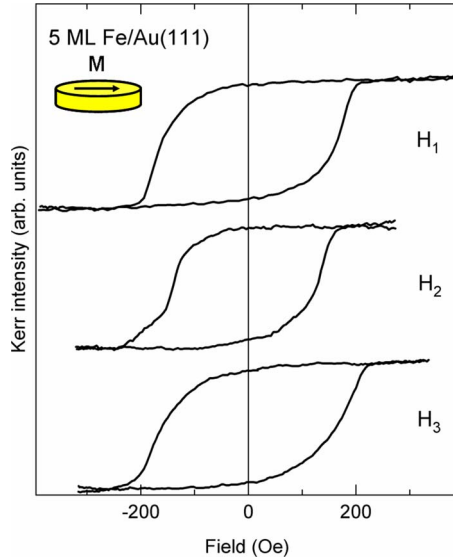
FIG. 5. (Color online) MOKE measurements of 5 ML of Fe on flat Au(111) with the field applied along different directions as depicted in Fig. 4. All measurements were performed at $T = 115$ K. The hysteresis curves are very similar to each other and the shape of the curves is different from an easy-magnetization behavior. The sweeping speed of the field was about 5 Oe/s.

rectangular shaped crystallites of bcc Fe(110).[17,49,50] Due to the different growth conditions for Fe on flat and vicinal Au(111) the orientation of the crystallites is different:[17] the crystallites on the flat Au(111) are predominantly oriented along all $\langle 01\bar{1} \rangle_{fcc}$ directions while for the crystallites formed on the vicinal Au(111) the growth along $[01\bar{1}]_{fcc}$, i.e., along the step edges, is not present.

The bcc(110) unit cells can fit in two different ways on the fcc(111) substrate. These are the Nishiyama-Wassermann (NW) (Refs. 51 and 52) and the Kurdjumov-Sachs (KS) (Ref. 53) orientations as sketched in Fig. 4. For the NW orientation the $[\bar{1}10]_{bcc}$ direction is parallel to the $\langle \bar{2}11 \rangle_{fcc}$ directions while in the case of the KS orientation the $[\bar{1}1\bar{1}]_{bcc}$ direction is parallel to the $\langle 01\bar{1} \rangle_{fcc}$ directions. An angle of 5.25° between the $[\bar{1}10]_{bcc}$ direction and the $\langle \bar{2}11 \rangle_{fcc}$ directions is present for the KS-oriented bcc(110) units cells. As can be seen in Fig. 4, the NW-growth mode results in three differently oriented bcc(110) unit cells for Fe on flat Au(111) and in two for vicinal Au(111). The growth in the KS mode results in six differently oriented bcc(110) unit cells for flat Au(111) and in four for vicinal Au(111).

The predominant orientation of the Fe crystallites results in a topography for Fe on flat Au(111) with a sixfold symmetry and on vicinal Au(111) in a twofold symmetry.[17] In order to study the influence of the different symmetries on the in-plane magnetization behavior, we performed MOKE measurements for Fe on flat Au(111) with the field applied along three different directions, namely, along $[01\bar{1}]_{fcc}$ ($H_1$), $[\bar{2}11]_{fcc}$ ($H_2$), and exactly in between $[\bar{1}\bar{1}2]_{fcc}$ and $[\bar{1}01]_{fcc}$ ($H_3$). As can be seen in Fig. 4, the chosen directions cover all important scenarios: magnetization along the closed-packed direction (i.e., along $[01\bar{1}]_{fcc}$), along the open-packed direc-
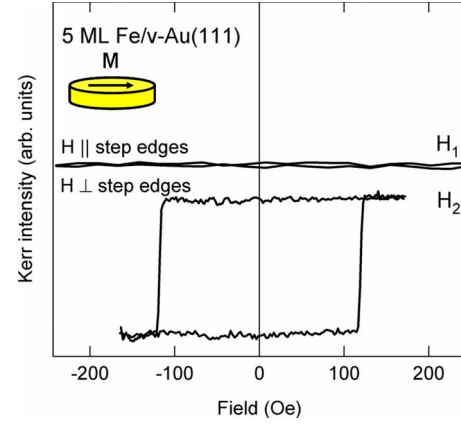


FIG. 6. (Color online) MOKE measurements of 5 ML of Fe on vicinal Au(111) with the field applied along different directions. All measurements were performed at $T = 115$ K. The sweeping speed of the field was about 5 Oe/s.

tion (i.e., along $[\bar{2}11]_{fcc}$), and magnetization along the direction exactly in between. For Fe on vicinal Au(111) we magnetized the sample along the step edges (i.e., along $[01\bar{1}]_{fcc}$) and perpendicular to the step edges (i.e., along $[\bar{2}11]_{fcc}$).

In the following we present the results obtained for longitudinal MOKE measurements at a temperature of $T = 115$ K for (i) Fe on flat Au(111) and (ii) Fe on vicinal Au(111): (i) the MOKE results for Fe on flat Au(111) are displayed in Fig. 5. The data were taken with the field applied along the different directions shown in Fig. 4. The hysteresis loops obtained for the three directions exhibit basically all the same shape, which is not squarelike. This indicates that neither field direction corresponds to an easy-magnetization direction.

(ii) The results of the MOKE measurements for Fe on vicinal Au(111) can be seen in Fig. 6. The data were obtained for the same directions of the applied fields as for the MOKE measurements of Fe on flat Au(111) except for the intermediate direction. We were not able to measure a Kerr intensity when the field is applied along the step edges (i.e., along $[01\bar{1}]_{fcc}$). When we apply the field perpendicular to the step edges (i.e., along $[\bar{2}11]_{fcc}$) we obtained a rectangular hysteresis curve. This is indicative of a hard and an easy-magnetization direction.

Our MOKE measurements suffer from the fact that we cannot ascribe the Kerr intensity to absolute values. For the presentation of our MOKE results in Figs. 3 and 5 we normalized the hysteresis curves to equal height. To obtain a quantitative measure of the influence of the topography on the magnetization behavior we employed spin-resolved PE. With spin-resolved PE it is possible to determine the spin polarization of the valence electrons which is a measure of the sample magnetization. This will be used in the following to determine the easy-magnetization direction.

The spin-resolved PE measurements were taken at a temperature of $T = 145$ K with the sample being magnetized in remanence. Thus, we applied the field along the same directions as for the MOKE measurements, namely $[\bar{2}11]_{fcc}$ ($H_1$), $[01\bar{1}]_{fcc}$ ($H_2$), and exactly in between $[\bar{1}\bar{1}2]_{fcc}$ and $[\bar{1}01]_{fcc}$
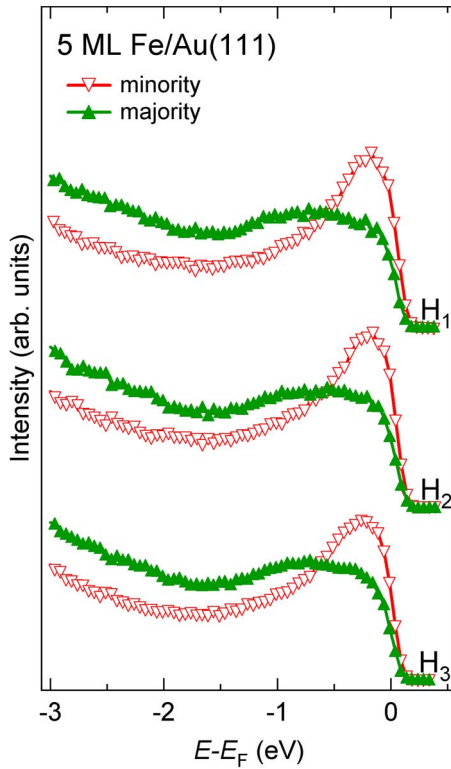
FIG. 7. (Color online) Spin-resolved PE measurements ($\hbar\omega$ =21.22 eV) of 5 ML Fe/Au(111) for normal electron emission in dependence of the direction in which the sample was remanently magnetized prior to the measurement.



FIG. 8. (Color online) Spin-resolved PE measurements ($\hbar\omega$ =21.22 eV) of 5 ML Fe/Au(23 25 25) for normal electron emission in dependence of the direction in which the sample was remanently magnetized prior to the measurement.

($H_3$) before measurement (see Fig. 4). The measurements were taken for normal electron emission at an excitation energy of $\hbar\omega$=21.22 eV. In the following we discuss the results for (i) Fe on flat Au(111) and (ii) Fe on vicinal Au(111).

(i) The spin-resolved PE measurements for Fe on flat Au(111) are shown in Fig. 7. We obtained spectra which are very similar to each other: near $E_F$ they exhibit a state in the majority- and minority-spin channels. At an energy of $E-E_F=-0.9$ eV a state is visible in the majority-spin channel. A majority-spin state at $E-E_F=-2.3$ eV is present with low intensity.

(ii) The spin-resolved PE measurements for Fe on vicinal Au(111) are shown in Fig. 8. When the field is applied along the step edges (i.e., along $[01\bar{1}]_{\text{fcc}}$) we obtained a spectrum which shows almost no spin polarization. When the field is applied perpendicular to the step edges (i.e., along $[\bar{2}11]_{\text{fcc}}$) we notice high spin polarization. Hardly any intensity in the majority-spin channel is present at $E_F$. Most of the intensity has minority-spin character. As in the case of Fe on flat Au(111) we observed a state at $E-E_F=-0.9$ eV which is present in the majority-spin channel. The state at $E-E_F=$ $-2.3$ eV in the majority-spin channel is also present. For a field applied under an angle of 45° toward the step edges the spin-resolved PE spectrum shows a reduced spin polarization over the entire energy range of the spectrum. This spectrum reminds us of the spectra for Fe on flat Au(111).

The MOKE and spin-resolved results provide a consistent picture. For Fe on flat Au(111) we observed a reduced rem-

anent magnetization in comparison with Fe on vicinal Au(111). The decay of the magnetization into different domains results in an additional intensity in the majority-spin channel near $E_F$ since some of the domains are not aligned to the quantization axis of the spin detection in the experiment. Consequently, the spin polarization is reduced. Due to the sixfold topography of Fe on flat Au(111) given by the crystallites we cannot magnetize the sample along an easy-magnetization direction. Thus, when we apply a field to the sample along a certain in-plane direction we measure a superposition of hysteresis loops stemming from differently oriented crystallites with their own magnetization reversals.
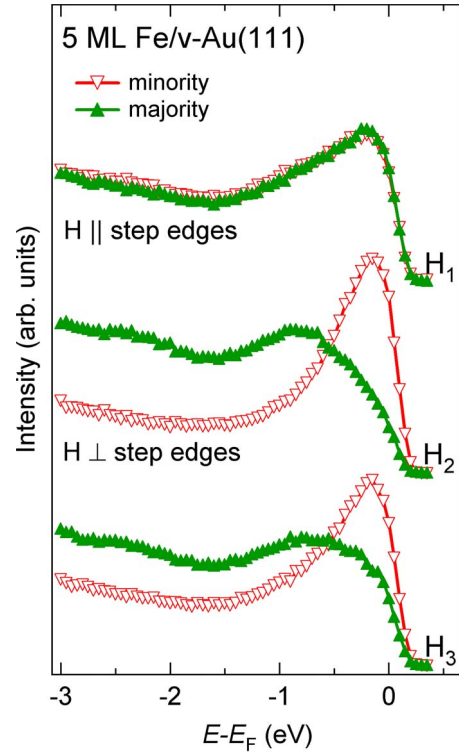
Fe on vicinal Au(111) exhibits a twofold topography due to the missing growth of the crystallites along the step edges. The magnetization behavior is therefore different to Fe on flat Au(111). No magnetic signal was measured with MOKE and spin-resolved PE when a field was applied along $[01\bar{1}]_{\text{fcc}}$. When we apply a field along $[\bar{2}11]_{\text{fcc}}$, which is perpendicular to $[01\bar{1}]_{\text{fcc}}$, we measure a rectangular shaped hysteresis curve. This indicates a one domain state with an easy-magnetization direction collinear to the applied field. The spin polarization is also larger for Fe on vicinal Au(111): we observed a maximum spin polarization for Fe on vicinal Au(111) of $(-60\pm2)\%$ close to $E_F$ and a maximum[54] spin polarization for Fe on flat Au(111) of $(-34\pm1)\%$. When the sample is magnetized at an angle of 45° toward the step edges, the spin polarization is reduced to a value of $(-37\pm2)\%$ at maximum value. This is strong evidence of an uniaxial anisotropy along $[\bar{2}11]_{\text{fcc}}$ because the factor between

−37% and −60% is 0.62 which is close to cos(45°).

It is a nontrivial task to predict the in-plane easy-magnetization direction, parallel or perpendicular to the step edges, in ultrathin ferromagnetic films on vicinal surfaces. From an experimental point of view, a first step would be to search for a systematics in the systems investigated so far. A number of system parameters might influence the magnetic anisotropy: geometry and crystalline properties of the deposited nanosized structures, combination of substrate and overlayer material, and interaction of both, details of the vicinal substrate including miscut angle, surface reconstruction, and coordination number of the step atoms. For Fe on vicinal Cu(111), Pt(997), and Au(23 25 25), crystallites with bcc(110) unit cells are present above a critical thickness in all three cases but the easy-magnetization direction is not the same: Fe on vicinal Cu(111) (Ref. 20) and Au(23 25 25) [this work] exhibit an easy-magnetization direction perpendicular to the step edges but for Fe on Pt(997) the easy-magnetization direction is parallel to the step edges.[21] Co on Au(455) shows an easy-magnetization direction perpendicular to the step edges[22] in agreement with our result for Fe on Au(23 25 25). Note that the substrates show significant differences in terrace width and surface reconstruction. Consequently, the geometry of the Co and Fe nanostructures is also different as well as the crystallography since Co does not show a phase transition to bcc. Thus, for similar structures like Fe on vicinal Cu(111), Pt(997), and Au(23 25 25), different in-plane easy-magnetization directions are observed while for different structures like Co on Au(455) in comparison with Fe on vicinal Cu(111) and Au(23 25 25), the same in-plane easy-magnetization direction was found. These examples show that it is not possible to predict the in-plane easy-magnetization direction from simple arguments. More sophisticated measurements of the local electronic structure and the relation between spin and orbital moments are required[20,55] in combination with detailed theoretical investigations.

## IV. SUMMARY AND CONCLUSION

In a previous work we found differences in the growth behavior of Fe on flat and vicinal Au(111).[17] In this work we studied the influence of the different growth behavior on the magnetic properties. A consequence of the impeded structural phase transition from fcc(111) to bcc(110) we observed an impeded SRT for Fe on vicinal Au(111) in comparison to Fe on flat Au(111), yet in a smaller thickness range than the structural phase transition. Combined with the results of Ref. 17 we conclude that the SRT takes place when the major part of the surface is covered with bcc(110) Fe crystallites while the structural phase transition starts at different locations on the sample. Thus, fcc(111) and bcc(110) regions of Fe can be observed on flat and vicinal Au(111) in coexistence.

With magneto-optical Kerr effect and spin-resolved photoemission we studied the in-plane magnetization behavior for bcc Fe(110) on flat and vicinal Au(111). The growth of Fe on flat Au(111) results in a topography which exhibits a sixfold symmetry. This orientation of the bcc(110) crystallites prohibits the existence of an overall easy-magnetization direction. For all studied in-plane magnetization directions we measured a superposition of different magnetization reversals leading to hysteresis curves with reduced remanent magnetization. With spin-resolved PE we found a reduced polarization for Fe on flat Au(111) in comparison with Fe on vicinal Au(111). For Fe on vicinal Au(111) we were able to clearly deduce an easy-magnetization direction which is perpendicular to the step edges of the substrate. Consequently, the MOKE curve is squarelike when the field is applied along this direction.

A quantitative knowledge of the remanent sample magnetization is essential for the correct analysis of spin-resolved PE data of the electronic structure. Our study shows that a defined one domain state can be achieved for Fe on Au(23 25 25) but not on flat Au(111).

*tobias.allmers@uni-muenster.de

[1] H. P. Oepen and J. Kirschner, Curr. Opin. Solid State Mater. Sci. **4**, 217 (1999).

[2] E. Williams, Surf. Sci. **299-300**, 502 (1994).

[3] F. J. Himpsel, J. E. Ortega, G. J. Mankey, and R. F. Willis, Adv. Phys. **47**, 511 (1998).

[4] H. J. Elmers, J. Hauschild, and U. Gradmann, J. Magn. Magn. Mater. **221**, 219 (2000).

[5] P. Gambardella, J. Phys.: Condens. Matter **15**, S2533 (2003).

[6] T. Jung, R. Schlittler, J. K. Gimzewski, and F. J. Himpsel, Appl. Phys. A: Mater. Sci. Process. **61**, 467 (1995).

[7] J. N. Crain and F. J. Himpsel, Appl. Phys. A: Mater. Sci. Process. **82**, 431 (2006).

[8] G. Ketteler and W. Ranke, J. Vac. Sci. Technol. A **23**, 1055 (2005).

[9] F. J. Himpsel, T. Jung, A. Kirakosion, J.-L. Lin, D. Y. Petrovylk, H. Rauser, and J. Viernow, MRS Bull. **24**, 20 (1999).

[10] J. Shen, R. Skomski, M. Klaua, H. Jenniches, S. Sundar Manoharan, and J. Kirschner, Phys. Rev. B **56**, 2340 (1997).

[11] F. Picaud, V. Pouthier, C. Ramseyer, and C. Girardet, Surf. Rev. Lett. **6**, 669 (1999).

[12] Ruihua Cheng, K. Yu. Guslienko, F. Y. Fradin, J. E. Pearson, H. F. Ding, Dongqi Li, and S. D. Bader, Phys. Rev. B **72**, 014409 (2005).

[13] P. Gambardella, M. Blanc, L. Bürgi, K. Kuhnke, and K. Kern, Surf. Sci. **449**, 93 (2000).

[14] S. Rousset, V. Repain, G. Baudot, Y. Garreau, and J. Lecoeur, J. Phys.: Condens. Matter **15**, S3363 (2003).

[15] M. Giesen and T. L. Einstein, Surf. Sci. **449**, 191 (2000).

[16] A. Mugarza, A. Mascaraque, V. Repain, S. Rousset, K. N. Alt-

mann, F. J. Himpsel, Yu. M. Koroteev, E. V. Chulkov, F. J. García de Abajo, and J. E. Ortega, Phys. Rev. B **66**, 245419 (2002).

[17] T. Allmers and M. Donath, New J. Phys. **11**, 103049 (2009).

[18] R. K. Kawakami, Ernesto J. Escorcia-Aparicio, and Z. Q. Qiu, Phys. Rev. Lett. **77**, 2570 (1996).

[19] J. Shen, M. Klaua, P. Ohresser, H. Jenniches, J. Barthel, Ch. V. Mohan, and J. Kirschner, Phys. Rev. B **56**, 11134 (1997).

[20] C. Boeglin, S. Stanescu, J. P. Deville, P. Ohresser, and N. B. Brookes, Phys. Rev. B **66**, 014439 (2002).

[21] D. Repetto, T. Y. Lee, S. Rusponi, J. Honolka, K. Kuhnke, V. Sessi, U. Starke, H. Brune, P. Gambardella, C. Carbone, A. Enders, and K. Kern, Phys. Rev. B **74**, 054408 (2006).

[22] J. H. Gao, Y. Girard, V. Repain, A. Tejeda, R. Belkhou, N. Rougemaille, C. Chacon, G. Rodary, and S. Rousset, Phys. Rev. B **77**, 134429 (2008).

[23] M. Budke, T. Allmers, M. Donath, and G. Rangelov, Rev. Sci. Instrum. **78**, 113909 (2007).

[24] D. H. Yu, C. Math, M. Meier, M. Escher, G. Rangelov, and M. Donath, Surf. Sci. **601**, 5803 (2007).

[25] J. Kirschner and R. Feder, Phys. Rev. Lett. **42**, 1008 (1979).

[26] J. Perdereau, J. P. Biberian, and G. E. Rhead, J. Phys. F: Met. Phys. **4**, 798 (1974).

[27] M. A. van Hove, R. J. Koestner, P. C. Stair, J. P. Bibérian, L. L. Kesmodel, I. Bartoš, and G. A. Somorjai, Surf. Sci. **103**, 189 (1981).

[28] Ch. Wöll, S. Chiang, R. J. Wilson, and P. H. Lippel, Phys. Rev. B **39**, 7988 (1989).

[29] J. V. Barth, H. Brune, G. Ertl, and R. J. Behm, Phys. Rev. B **42**, 9307 (1990).

[30] S. Shiraki, H. Fujisawa, M. Nantog, and M. Kawai, Appl. Surf. Sci. **237**, 284 (2004).

[31] M. T. Kief and W. F. Egelhoff, Phys. Rev. B **47**, 10785 (1993).

[32] H. Glatzel, T. Fauster, B. M. U. Scherzer, and V. Dose, Surf. Sci. **254**, 58 (1991).

[33] J. Thomassen, F. May, B. Feldmann, M. Wuttig, and H. Ibach, Phys. Rev. Lett. **69**, 3831 (1992).

[34] I. Horcas, R. Fernández, J. M. Gómez-Rodríguez, J. Colchero, J. Gómez-Herrero, and A. M. Baro, Rev. Sci. Instrum. **78**, 013705 (2007).

[35] J.-J. Yeh and I. Lindau, At. Data Nucl. Data Tables **32**, 1 (1985).

[36] The increase in intensity at $E - E_F \approx -2.3$ eV stems from the deposited Fe. This is revealed by the spin-resolved PE results of Fig. 8.

[37] H. Fujisawa, S. Shiraki, M. Nantoh, and M. Kawai, Surf. Interface Anal. **37**, 124 (2005).

[38] M. P. Seah and W. A. Dench, Surf. Interface Anal. **1**, 2 (1979).

[39] D. P. Pappas, K.-P. Kämper, B. P. Miller, H. Hopster, D. E. Fowler, C. R. Brundle, A. C. Luntz, and Z.-X. Shen, Phys. Rev. Lett. **66**, 504 (1991).

[40] M. Getzlaff, J. Bansmann, and G. Schönhense, Solid State Commun. **87**, 467 (1993).

[41] F. Passek, M. Donath, and K. Ertl, J. Magn. Magn. Mater. **159**, 103 (1996).

[42] O. Toulemonde, V. Petrov, A. Nait Abdi, and J. P. Bucher, J. Appl. Phys. **95**, 6565 (2004).

[43] J. Xu, M. A. Howson, P. Hucknall, B. J. Hickey, R. Venkataraman, C. Hammond, M. J. Walker, and D. Greig, J. Appl. Phys. **81**, 3908 (1997).

[44] S. Araki, T. Takahata, H. Donomae, T. Okuyama, and T. Shinjo, in *Growth, Characterization and Properties of Ultrathin Magnetic Films and Multilayers*, edited by B. T. Jonker, J. P. Heremans, and E. E. Marinero, MRS Symposia Proceedings No. 151 (Materials Research Society, Pittsburgh, 1989), p. 123.

[45] G. Lugert, W. Robl, L. Pfau, M. Brockmann, and G. Bayreuther, J. Magn. Magn. Mater. **121**, 498 (1993).

[46] Since only one SRT is present for the system Fe on flat Au(111) and since the SRT is correlated to the phase transition fcc(111) to bcc(110), we do not expect a second SRT for Fe on vicinal Au(111) either.

[47] S. Shiraki, H. Fujisawa, T. Nakamura, T. Muro, M. Nantoh, and M. Kawai, Phys. Rev. B **78**, 115428 (2008).

[48] A. Biedermann, W. Rupp, M. Schmid, and P. Varga, Phys. Rev. B **73**, 165418 (2006).

[49] B. Voigtländer, G. Meyer, and N. M. Amer, Surf. Sci. Lett. **255**, L529 (1991).

[50] J. Stroscio, D. Pierce, R. Dragoset, and P. First, J. Vac. Sci. Technol. A **10**, 1981 (1992).

[51] Z. Nishiyama, K. Shimizu, and K. Sugino, Acta Metall. **9**, 620 (1961).

[52] E. F. Wassermann and H. P. Jablonski, Surf. Sci. **22**, 69 (1970).

[53] G. Kurdjumov and G. Sachs, Z. Phys. **64**, 325 (1930).

[54] For a film thickness of 10 ML we found a maximum spin polarization of $(-67 \pm 2)\%$ for a magnetization perpendicular to the step edges.

[55] S. Rusponi, T. Cren, N. Weiss, M. Epple, P. Buluschek, L. Claude and H. Brune, Nature Mater. **2**, 546 (2003).